Chapter 3
Model of the Robotic Elements

3.1 Tethering Link

In this book we address the control problem of tethered aerial vehicles from the most generic point of view, deriving general and fundamental theoretical results that can be then easily applied to several practical cases. For this reason, in Sect. 4.3 we consider the aerial vehicle tethered to a moving platform by a *generic link*, either a cable, a chain, a rope, a bar or a strut. All the considered links can be divided into three major categories, schematically represented in Fig. 3.1:

(a) Links that can be *only stretched*, i.e., that can support *only tensions*. To this category fall all the types of cable-like link, e.g., a chain, a rope, etc.
(b) Links that can be *only compressed*, i.e., that can support *only compressions*. To this category fall all the types of strut-like link, such as a pneumatic suspension.
(c) Links that can be *both stretched and compressed*, i.e., that can support *both tensions and compressions*. To this category fall all the types of bar-like link, such as a beam, a pole, etc.

The main variables that describe a generic link are: the position of the edges given by the vectors $\mathbf{p}_1 \in \mathbb{R}^3$ and $\mathbf{p}_2 \in \mathbb{R}^3$, the unstressed length $l_0 \in \mathbb{R}_{>0}$ and the intensity of the internal force $f_L \in \mathbb{R}$. Other equivalent but still meaningful variables can be defined: the length of the link $l = \|\mathbf{p}_1 - \mathbf{p}_2\| \in \mathbb{R}$ and the normalized axis of the link $\mathbf{d} = (\mathbf{p}_1 - \mathbf{p}_2)/l \in \mathbb{R}^3$. Figure 3.2 shows the main variables describing a link.

When the link is pulled the internal force is called *tension* and $f_L > 0$, whereas when it is compressed the internal force is called *compression* and $f_L < 0$. When $f_L = 0$ the link is *slack*. The easiest way to model the link is as a hybrid system with two states: slack or non-slack, i.e., taut/compressed. When the link is slack and $f_L = 0$, the length of the link can be: (a) $l \leq l_0$ for a cable-like link; (b) $l \geq l_0$ for a strut-like link; and (c) $l = l_0$ for a bar-like link. In this condition the two ends of the cable are treated as two independent systems, as done in [1, 2]. However, we are not interested in this case since we shall design a controller that will keep away the system from the slack state for the cable and strut-like link cases.

M. Tognon and A. Franchi, *Theory and Applications for Control of Aerial Robots in Physical Interaction Through Tethers*, Springer Tracts in Advanced Robotics 140,
https://doi.org/10.1007/978-3-030-48659-4_3

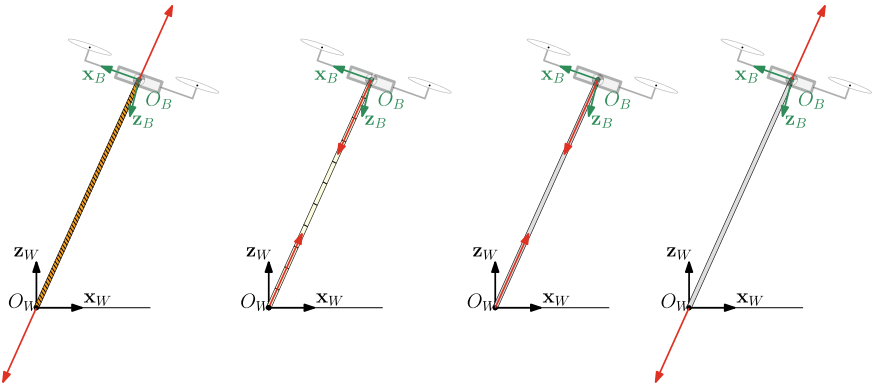

(a) Cable-like link can be only stretched.

(b) Strut-like link can be only compressed

(c) Bar-like link can be compressed (left) and stretched (right)

Fig. 3.1 Three type of considered link. The red arrows indicate the external forces (or reaction forces) that stretch or compress the link, according to the category

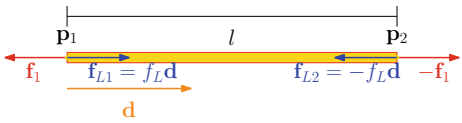

Fig. 3.2 Schematic representation of a general link and its main variables

On the other hand, when the cable is taut or compressed, i.e., $f_L \neq 0$, we assume that the length of the link remain constant independently from the internal force, $l = l_0$. This is equivalent to assume that, in the domain of interest, a non-slack link is a rigid element whose elasticity and deformations are negligible. This assumption is very common in the related literature review [3, 4], and is valid as soon as the maximum internal force of interest is much smaller than the stiffness coefficient of the link. Under this assumption we have that the internal force at the two ends are opposite, and always along the link axis, $\mathbf{f}_{L2} = -\mathbf{f}_{L1} = -f_L\mathbf{d}$.

As also commonly done in the related state of the art, we assume negligible mass and inertia of the link with respect to the one of the aerial vehicle. Also this assumption is easily met using very lightweight links like kite cables or link structures based on carbon fiber.

Nevertheless, one could use more complex models to describes all the previously neglected effects. For example a *spring-damper* system can be used to better describe the deformations of the link subjected to external forces. According to the particular type of link, even more complex and accurate models could be employed. For example, in the case of a cable-like link, one can use a *Standard Linear Solid model* (SLS) [5–7] consisting of a series of a spring and a parallel of spring-damper. This model better describes the response delay due to the relatively slow microscopic deformation process acting in the rope when some external forces are stretching it. Furthermore, in order to also model flexibility of cables and the bending due to grav-

ity, one could model it by a *finite element approximation* [7]. It consists on modeling the link as a chain of elements, i.e., as a finite number of smaller links connected in series, as done in [8, 9].

Although the previously mentioned models better describe the real behaviors of the considered links, actually, the effects that they additionally describe with respect to the simple mass-less rigid body model, are negligible in the domain of interest. Furthermore, they are specific only for certain type of links. On the other hand, the mass-less rigid body model is a general model that can be applied to the several classes of link previously presented. Thus it is more suitable for the aimed control objectives. This is why, for the sake of designing control and observer methods, we choose this model to derive the equations of motion of the considered tethered aerial vehicle (see Sect. 4.3). Nevertheless, in Sect. 5.4.2 we shall show that the proposed methods based on the mass-less rigid body model are robust enough also considering more accurate non-ideal models.

3.2 Unidirectional Thrust Vehicles

As usual, we start by defining an inertial world frame $\mathcal{F}_W = \{O_W, \mathbf{x}_W, \mathbf{y}_W, \mathbf{z}_W\}$ where O_W is its origin, placed arbitrarily, and $(\mathbf{x}_W, \mathbf{y}_W, \mathbf{z}_W)$ are the orthogonal unit vectors. We consider $\mathbf{z}_W$ parallel and opposite to the gravity vector. Then we define the body frame $\mathcal{F}_R = \{O_R, \mathbf{x}_R, \mathbf{y}_R, \mathbf{z}_R\}$ rigidly attached to the vehicle and centered in O_R, the vehicle CoM. We consider $\mathbf{z}_R$ parallel and opposite to the total thrust vector. The position of O_R and orientation of $\mathcal{F}_R$ w.r.t. $\mathcal{F}_W$ are described by the vector $\mathbf{p}_R \in \mathbb{R}^3$ and the rotation matrix $\mathbf{R}_R \in \mathsf{SO}(3)$, respectively. Then we denote by the vector $\boldsymbol{\omega}_R \in \mathbb{R}^3$ the angular velocity of $\mathcal{F}_R$ w.r.t. $\mathcal{F}_W$ and expressed in $\mathcal{F}_R$. The variables describing the vehicle are depicted in Fig. 3.3.

As already announced in Sect. 2.1.3, the vehicle is modeled as a rigid body with mass $m_R \in \mathbb{R}_{>0}$ and moment of inertia about O_R, defined w.r.t. $\mathcal{F}_R$, described by the

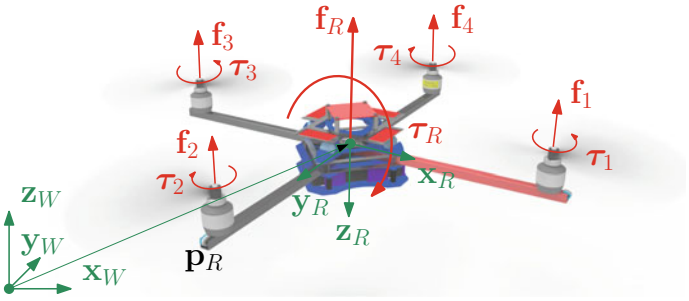

Fig. 3.3 Schematic representation of a collinear multirotor and its main quantitites. Although the vehicle is represented as a quadrotor, actually it can be any collinear multirotor, such as an hexarotor, octorotor, etc.

positive definite matrix $\mathbf{J}_R \in \mathbb{R}^{3\times3}_{>0}$ [10, 11]. The motion of the vehicle is controlled by the coordinated action of four control inputs: *(i)* $f_R \in \mathbb{R}_{\geq 0}$ is the *intensity of the total thrust* applied in O_R such that $\mathbf{f}_R = -f_R\mathbf{z}_R$, which generates translational motion, and *(i)* $\boldsymbol{\tau}_R = [\tau_{Rx} \ \ \tau_{Ry} \ \ \tau_{Rz}]^\top \in \mathbb{R}^3$ is the *total moment* applied to $\mathcal{F}_R$ and expressed in $\mathcal{F}_R$, which generates rotational motion.

Similarly to Sect. 2.1.3, the dynamics of the system is computed applying the Newton-Euler equations, thus obtaining $\dot{\mathbf{R}}_R = \mathbf{R}_R\boldsymbol{\Omega}_R$, and

$$m_R\ddot{\mathbf{p}}_R = -m_R g\mathbf{e}_3 - f_R\mathbf{R}_R\mathbf{e}_3 \tag{3.1a}$$

$$\mathbf{J}_R\dot{\boldsymbol{\omega}}_R = -\boldsymbol{\omega}_R \times \mathbf{J}_R\boldsymbol{\omega}_R + \boldsymbol{\tau}_R. \tag{3.1b}$$

This model is general and well describes the dynamics of the majority of unidirectional thrust aerial vehicles as ducted fan and multirotors vehicles with four or more rotors. Indeed, (3.1) encapsulates all the nonlinearities and the underactuation of unidirectional-thrust aerial vehicles. One can notice how, in order to apply a certain acceleration, the vehicle has to be oriented such that the total thrust vector is oriented such to ensure an acceleration that is equal to the given acceleration plus the gravity compensation. This shows the coupling between translational and rotational dynamics.

Thanks to its generality, we will use this model to describe the dynamics of the aerial vehicles considered in the following. However, how to practically generate the total thrust and the torque will be treated in the following section.

3.3 Actuators

3.3.1 Thrusters

In this thesis we consider a particular class of unidirectional-thrust aerial vehicles. We consider aerial vehicles that generate the total thrust and torque by the aerodynamic forces and moments in turn generated by multiple collinear propellers. In practice, a model for those systems is needed to map total thrust and torque into the real control inputs.

Let us assume that the vehicle is endowed with $n \in \mathbb{N}_{\geq 4}$ thrusters. The generic i-th thruster is rigidly attached to the main frame oriented as $-\mathbf{z}_R$, and its position is given by the vector $\mathbf{b}_i \in \mathbb{R}^3$ with respect to $\mathcal{F}_R$. It is composed by a pair of brushless-motor plus propeller. Making the propeller spin at a certain velocity $w_i \in \mathbb{R}_{\geq 0}$, it can produce a force $f_i\mathbf{z}_R$, whose intensity is equal to $f_i = c_f w_i^2$, where $c_f \in \mathbb{R}_{>0}$ is called *lift factor* and depends on the aerodynamic properties of the propeller blades [10, 12–15]. When a propeller is spinning, the resistance of the air generates some horizontal forces on the blade, as well. Those drag forces, multiplied by the momentum arm and integrated over the rotor, generate a moment about the rotor shaft, that in the aerial robotics community is normally called *drag moment*. A reaction torque acts

on the rotor in the opposite direction of rotation of the propeller. The latter in turn generates a torque on the main frame of the vehicle that results to be proportional to the square of the propeller angular velocity, i.e., $\boldsymbol{\tau}_i = c_i c_\tau w_i^2 \mathbf{e}_3$, where *(i)* $c_i = 1$ ($c_i = -1$) if the i-th propeller angular velocity vector has the same direction of $\mathbf{z}_R$ ($-\mathbf{z}_R$), i.e., the propeller spins CCW (CW) when watched from its top; *(ii)* $c_\tau \in \mathbb{R}_{>0}$ also depends on the aerodynamic properties of the propeller.

Finally the total thrust and torque applied to the vehicle frame are given by:

$$f_R = \sum_{i=1}^{n} c_f w_i^2 \tag{3.2a}$$

$$\boldsymbol{\tau}_R = \sum_{i=1}^{n} (c_f \mathbf{b}_i \times \mathbf{e}_3 + c_i c_\tau \mathbf{e}_3) w_i^2. \tag{3.2b}$$

In particular, for a quadrotor-like vehicle where, $n = 4$, $\mathbf{b}_i = b[c_{\alpha_i} \;\; s_{\alpha_i} \;\; 0]^\top$ with $b \in \mathbb{R}_{>0}$ and $\alpha = (i-1)\pi/2$, $c_i = (-1)^i$ and $i = 1, \ldots, 4$, we have that

$$\begin{bmatrix} f_R \\ \boldsymbol{\tau}_R \end{bmatrix} = \underbrace{\begin{bmatrix} c_f & c_f & c_f & c_f \\ 0 & -c_f b & 0 & c_f b \\ c_f b & 0 & -c_f b & 0 \\ -c_\tau & c_\tau & -c_\tau & c_\tau \end{bmatrix}}_{\mathbf{F}} \begin{bmatrix} w_1^2 \\ w_2^2 \\ w_3^2 \\ w_4^2 \end{bmatrix}. \tag{3.3}$$

Notice that the allocation matrix $\mathbf{F}$ is square and full rank, thus always invertible. Once the desired total thrust and torque are computed, we can compute the spinning velocity of each propeller that should be actuated to generate the desired control action just by inverting (3.3).

In particular conditions such as strong wind or at a very high speed, other gyroscopic and aerodynamic effects such as drag and blade flapping should be considered [10, 12, 16]. Additional aerodynamic effects are the ground and ceiling effects that arise whenever the vehicle flies close to a surface. However, as normally done in the related literature, we do not consider those effects since they are negligible in the domain of interest.

Furthermore, notice that the actuation model presented in (3.2) assumes that the motors can actuate the desired spinning velocity instantaneously. Nevertheless, changing the spinning velocity instantaneously would require an infinite torque that is obviously practically unfeasible. One should instead add to (3.2) the dynamics of the motor, both from a mechanic and electronic point of view [17], together with the dynamics of the electronic speed controller (ESC). A system identification of the overall closed loop system can be done to estimate the model parameters. Nevertheless, for control design purposes, we can assume that the spinning velocity variations are limited in the domain of interest. Under this assumption and thanks to the employed brushless controller [18] that guarantees minimal response times, model (3.2) results a good approximation of the real behavior. On the other hand,

more complex and realistic models, such as the ones mentioned before, can be used for the validation of the theoretical results in a more realistic condition (see Chap. 5).

3.3.2 *Link Actuator*

In this thesis the link actuator is modeled as a cylinder that transform the rotational motion of a motor to a translational motion, namely the variation of the link length. In particular, in the case of a cable-like link, the cable is rolled on the cylinder, while in the case of a bar-like link, the cylinder is a gear mechanism that moves back and forward the link changing its length. The cylinder is moved by a motor that exerts an input torque $\tau_W \in \mathbb{R}$ about the longitudinal axis of the cylinder. We assume that the rotational inertia and radius of the link actuator, denoted by $J_W \in \mathbb{R}_{>0}$ and $r_W \in \mathbb{R}_{>0}$, respectively, are constant in the domain of interest. The dynamic of the link actuator is

$$J_W \ddot{\vartheta}_W = \tau_W + f_L r_W, \tag{3.4}$$

where $\ddot{\vartheta}_W$ is the angular acceleration of the actuator. Since we are more interested in the dynamics of the link length, we can easily describe it from (3.4). Assuming no backlash we can write $l = r_W \vartheta_W$, thus

$$\bar{J}_W \ddot{l} = \bar{\tau}_W + f_L, \tag{3.5}$$

where $\bar{J}_W = J_W / r_W^2$ and $\bar{\tau}_W = \tau_W / r_W$.

According to the real implementation some assumptions, like the constant inertia and radius might not hold anymore. However the model can be easily changed accordingly.

3.4 Sensory Setup

To control the previous modeled aerial vehicles the knowledge of the state is needed in most of the cases. In other words, the position, the linear velocity, the attitude and the angular velocity of the vehicle have to be estimated from the available sensors, in order to then compute the control action.

The most basic sensor available on practically all vehicles is the *inertial measurement unit* (IMU) [10, 19, 20]. It normally consists of an 3-axes accelerometer and a 3-axes gyroscope. The first measures the so call "specific acceleration", namely the acceleration of the vehicle with respect to the body frame minus the gravity vector. Defining $\mathbf{w}_{acc} \in \mathbb{R}^3$ the measure coming from the accelerometer, and assuming that the IMU is calibrated, centered at O_R and its axes are aligned with the ones of $\mathcal{F}_R$, we have that:

$$\mathbf{w}_{acc} = \mathbf{R}_R^\top(\ddot{\mathbf{p}}_R + g\mathbf{e}_3). \tag{3.6}$$

On the other hand, the gyroscope, whose measurements are defined by the vector $\mathbf{w}_{gyr} \in \mathbb{R}^3$, directly measures, under the same assumptions, the angular velocity of $\mathcal{F}_R$ with respect to $\mathcal{F}_W$ expressed in $\mathcal{F}_R$:

$$\mathbf{w}_{gyr} = \boldsymbol{\omega}_R. \tag{3.7}$$

These two quantities are not enough to estimate the full time-varying attitude, because the rotation along $\mathbf{z}_R$, is not observable in hovering conditions [10, 21]. This is why the IMU is often equipped with a *magnetomer* that measures the ambient magnetic field with respect to the body frame. In the absence of disturbances, the latter corresponds to the known Earth's magnetic field defined by the vector $\mathbf{h}^W \in \mathbb{R}^3$. Under this assumption, the magnetometer measurement, $\mathbf{w}_{mag} \in \mathbb{R}^3$, is equal to:

$$\mathbf{w}_{mag} = \mathbf{R}_R^\top \mathbf{h}^W. \tag{3.8}$$

The combination of the previous three sensors is in principle sufficient to estimate the rotational part of the state [22–25], i.e., the attitude and the angular velocity.

For estimating the rest of the state, i.e., the position and the translational velocity, some other exteroceptive sensors are usually needed. Some examples are motion capture system (MoCap) for precise indoor localization, GPS and differential GPS for outdoor environments, and various type of cameras for outdoor GPS-denied environments. Since the design of new localization methods using those kind of exteroceptive sensors is not the focus of this thesis, we will model them as a direct measurement of the configuration of the robot. Thus, defining $\mathbf{w}_{ext}$ the output measurement, we have that:

$$\mathbf{w}_{ext} = (\mathbf{p}_R, \mathbf{R}_R). \tag{3.9}$$

The authors of [10] present the most popular methods to fuse all the mentioned sensors in order to finally obtain a precise estimation of the full state.

However, in Chap. 4 (see Sects. 4.7 and 4.8) we shall show that for a tethered aerial vehicle, those exteroceptive sensors are not needed to estimate the full state of the system. Indeed, we found that, thanks to the link constraint, in a 2D environment only an IMU is enough to retrieve an estimation of the fulls state (see Sect. 4.8). On the other hand, in the 3D environment, we found that the minimal sensory setup consists of a standard IMU and magnetometer, plus only some encoders to measure the attitude of the link and its length (if not constant).

In order to model the measurement of an encoder let us define two frames $\mathcal{F}_1 = \{O_1, \mathbf{x}_1, \mathbf{y}_1, \mathbf{z}_1\}$ and $\mathcal{F}_2 = \{O_2, \mathbf{x}_2, \mathbf{y}_2, \mathbf{z}_2\}$ such that $O_1 = O_2$ and $\mathbf{x}_1 = \mathbf{x}_2$. Then we have that:

$$\mathbf{w}_{enc} = \theta, \tag{3.10}$$

where $\theta \in \mathbb{R}$ is the angle to make $\mathcal{F}_2$ coincide with $\mathcal{F}_1$ rotating it about $\mathbf{y}_1$.

The models presented so far are the ideal ones and they will be used in the following to design deterministic and almost globally convergent nonlinear observers. However, in practice every sensor is affected by noise and biases. We will then rely on the proven robustness of the designed observer to deal with those non-idealities (see Chap. 5). Another approach would be to design a stochastic estimators that deals with noisy measurements. However they are normally based on linear approximation of the models and therefore they are not globally convergent.

References

1. Sreenath, K., Kumar, V.: Dynamics, control and planning for cooperative manipulation of payloads suspended by cables from multiple quadrotor robots. In: Robotics: Science and Systems, Berlin, Germany, June (2013)
2. Sreenath, K., Michael, N., Kumar, V.: Trajectory generation and control of a quadrotor with a cable-suspended load-a differentially-flat hybrid system. In: 2013 IEEE International Conference on Robotics and Automation (ICRA), pp. 4888–4895. IEEE (2013)
3. Lupashin, S., D'Andrea, R.: Stabilization of a flying vehicle on a taut tether using inertial sensing. In: 2013 IEEE/RSJ International Conference on Intelligent Robots and Systems, pp. 2432–2438, Tokyo, Japan, Nov (2013)
4. Nicotra, M.M., Naldi, R., Garone, E.: Nonlinear control of a tethered UAV: the taut cable case. Automatica **78**, 174–184 (2017)
5. Sandino, L.A., Bejar, M., Kondak, K., Ollero, A.: Advances in modeling and control of tethered unmanned helicopters to enhance hovering performance. J. Intell. Robot. Syst. **73**(1–4), 3–18 (2014)
6. Liu, H.P., Anderson, D.L., Kanamori, H.: Velocity dispersion due to anelasticity; implications for seismology and mantle composition. Geophys. J. Int. **47**(1), 41–58 (1976)
7. Zienkiewicz, O.C., Taylor, R.L.: The Finite Element Method for Solid and Structural Mechanics. Elsevier (2005)
8. Lee, T.: Geometric controls for a tethered quadrotor UAV. In: 2015 54th IEEE Conference on Decision and Control (CDC), pp. 2749–2754, Osaka, Japan, Dec (2015)
9. Goodarzi, F.A., Lee, T.: Stabilization of a rigid body payload with multiple cooperative quadrotors. J. Dyn. Syst. Meas. Control **138**(12), 121001–121001–17 (2016)
10. Mahony, R., Kumar, V., Corke, P.: Multirotor aerial vehicles: modeling, estimation, and control of quadrotor. IEEE Robot. Autom. Mag. **19**(3), 20–32 (2012)
11. Hua, M.-D., Hamel, T., Morin, P., Samson, C.: A control approach for thrust-propelled underactuated vehicles and its application to VTOL drones. IEEE Trans. Autom. Control **54**(8), 1837–1853 (2009)
12. Hamel, T., Mahony, R., Lozano, R., Ostrowski, J.: Dynamic modelling and configuration stabilization for an X4-Flyer. In: 15th IFAC World Congress, pp. 217–222, Barcelona, Spain (2002)
13. Pounds, P.E., Mahony, R., Corke, P.: Modeling and control of a large quadrotor robot. Control Eng. Pract. **18**(7), 691–699 (2010)
14. Valavanis, K.P.: Advances in Unmanned Aerial Vehicles: State of the Art and the Road to Autonomy. Intelligent Systems, Control and Automation: Science and Engineering, vol. 33. Springer (2007)
15. Pucci, D., Hamel, T., Morin, P., Samson, C.: Nonlinear control of aerial vehicles subjected to aerodynamic forces. In: 2013 IEEE 52nd Annual Conference on Decision and Control (CDC), pp. 4839–4846. IEEE (2013)

16. Faessler, M., Franchi, A., Scaramuzza, D.: Differential flatness of quadrotor dynamics subject to rotor drag for accurate tracking of high-speed trajectories. IEEE Robot. Autom. Lett. **3**(2), 620–626 (2018)
17. Bangura, M., Mahony, R.: Thrust control for multirotor aerial vehicles. IEEE Trans. Robot. **33**(2), 390–405 (2017)
18. Franchi, A., Mallet, A.: Adaptive closed-loop speed control of BLDC motors with applications to multi-rotor aerial vehicles. In: 2017 IEEE International Conference on Robotics and Automation, pp. 5203–5208, Singapore, May (2017)
19. Ahmad, N., Ghazilla, R.A.R., Khairi, N.M., Kasi, V.: Reviews on various inertial measurement unit (IMU) sensor applications. Int. J. Signal Process. Syst. **1**(2), 256–262 (2013)
20. Martin, P., Salaün, E.: The true role of accelerometer feedback in quadrotor control. In: 2010 IEEE International Conference on Robotics and Automation, pp. 1623–1629, Anchorage, AK, May (2010)
21. Leishman, R.C., Macdonald, J.C., Beard, R.W., McLain, T.W.: Quadrotors and accelerometers: state estimation with an improved dynamic model. IEEE Control Syst. **34**(1), 28–41 (2014)
22. Mahony, R., Hamel, T., Pflimlin, J.-M.: Nonlinear complementary filters on the special orthogonal group. IEEE Trans. Autom. Control **53**(5), 1203–1218 (2008)
23. Kraft, E.: A quaternion-based unscented kalman filter for orientation tracking. In: Proceedings of the Sixth International Conference of Information Fusion, vol. 1, pp. 47–54 (2003)
24. Scandaroli, G.G., Morin, P., Silveira, G.: A nonlinear observer approach for concurrent estimation of pose, IMU bias and camera-to-IMU rotation. In: 2011 IEEE/RSJ International Conference on Intelligent Robots and Systems (IROS), pp. 3335–3341 (2011)
25. Scandaroli, G.G., Morin, P.: Nonlinear filter design for pose and IMU bias estimation. In: 2011 IEEE International Conference on Robotics and Automation (ICRA), pp. 4524–4530 (2011)